Key words: XAS, Chromium species, adsorption mechanism, biomass/biochar, water remediation

1. Introduction

Chromium is a common contaminant in surface and ground waters that is mainly originated from electroplating, leather tanning, and textile industries processes (Jobby et al., 2018; Markiewicz et al., 2015; Wang et al., 2019). Trivalent, Cr(III), and hexavalent, Cr(VI), oxidation states are the two main valence states found in polluted water (Miretzky and Cirelli, 2010; Sarin et al., 2006). Cr(VI) is hundreds of times more toxic than Cr(III) and it may cause carcinogenesis, mutation or teratogenesis to living organisms (Nath and Kumar, 1988; Sterritt and Lester, 1984). This is the reason why Cr(VI) has been identified as a top-priority hazardous pollutant to be addressed in water remediation (Pellerin and Booker, 2000). Therefore, it is of great significance to develop cost-effective and eco-friendly techniques to remove Cr from industrial wastewater before being released to the environment.

Numerous physical and chemical separation techniques are being used to remove heavy metals, such as solvent extraction, ion-exchange, adsorption, membrane filtration, electrochemical treatment technologies (Demirbas, 2008; GracePavithra et al., 2019; Pradhan et al., 2017; Wan Ngah and Hanafiah, 2008). Among the conventional techniques for removing pollutants from water, adsorption methods are considered to be the most advantageous due to their high efficiency, low cost and ease handling (Inyang et al., 2012; Tan et al., 2015). For instance, lignocellulosic residues (including wood and agricultural residues), due to the higher amount of functional groups (e.g. carboxyl) on the surface, have proven to be cost-effective adsorbents for removing Cr (Gode et al., 2008; Miretzky and Cirelli, 2010; Zhao et al., 2019). In addition, there are currently a large amount of wood biomass residues that have no market value and often become an environmental problem

if not disposed properly. In addition, biochar materials obtained after pyrolyzing biomass are also interesting sorbent materials due to their high surface area and high adsorption capacity for heavy metals. The greater concentration of mineral elements (K, Ca, Mg, P) in the in biochar respect to the original biomass, mainly due to the formation of biomass ash during pyrolysis, can promote adsorption of Cr^{3+} via cation exchange (Bagreev et al., 2001; Hossain et al., 2011; Sun et al., 2014; Zhao et al., 2017). Hence, the use of wood biomass and biochar derivatives as sorbents for water remediation have emerged as ideal solution for achieving a valorization of these forestry and industrial residues (Álvarez-Álvarez et al., 2018; Braghiroli and Passarini, 2020) and biochars byproducts obtained from the energy-related applications (Heredia Salgado et al., 2020; Littlejohns et al., 2020). On the other hand, metal oxides and metal oxide nanoparticles have been extensively used for heavy metal adsorption (Ray and Shipley, 2015). Among them, TiO_2 has exhibited high adsorption for Cr (Weng et al., 1997), good regenerative potential (Hu and Shipley, 2013) and outstanding photocatalytic properties under UV/Vis light that have been applied for Cr(VI) reduction (Wang et al., 2004). Thus, loading TiO_2 particles into cost-effective porous biosorbents used as a support is an approach that can prevent the particle aggregation occurring when the particles are suspended in liquid media. This is expected to improve the adsorption capabilities of the initial material.

In this work, we have studied the Cr adsorption on pine wood biomass (Pine) since it is a very abundant waste, and on two derived materials which are biochar obtained by gasification pyrolysis (PG) and pine loaded with TiO_2 (Pine/TiO_2). The main objective of this work is to understand the adsorption capabilities of each chromium species, Cr(III) and Cr(VI), by each sorbent material. In order to get a better understanding of the nature of the interactions between Cr and the sorbent

materials at molecular level, X-ray absorption spectroscopy (XAS) has been used to study the chemical environment around the adsorbed Cr atoms.

2. Materials and Methods

2.1 Chemical and reagents

All the chemicals used were analytical grade. A 1000 mg/L concentration of stock aqueous solution was prepared for Cr(III) and Cr(VI) species by dissolving the appropriated amounts of chromium nitrate nonahydrate, $Cr(NO_3)_3 \cdot 9H_2O$, and potassium dichromate, $K_2Cr_2O_7$, respectively, in acidic media, pH 1.0 (with 0.1 M of HNO_3). Both reagents had a purity of 99% and were obtained from Panreac (Barcelona, Spain). Ethanol (C_2H_6O, 97% v/v), nitric acid (HNO_3, 65% v/v) and hydrochloric acid (HCl, 37% v/v) all were purchased from Panreac. Titanium(IV) butoxide ($C_{16}H_{36}O_4Ti$, 97% v/v) was obtained from Sigma-Aldrich (St. Louis, USA).

2.2 Sorbent materials description and synthesis

Pine, Pine/TiO_2 and PG materials were selected as sorbent materials for Cr removal from aqueous solutions following the motivation described in the Introduction section. Pine biomass and PG biochar were kindly provided by the Centre for Research on Ecology and Forestry Applications (CREAF, Barcelona, Spain). As has been previously reported (Marks et al., 2016, 2014), PG biochar was obtained from Pine (*Pinus pinaster* and *Pinus radiata)* biomass wood chip from an industrial gasification reactor. Production conditions at the facility ranged from 600 to 900 ^oC with an approximate holding time of 10 s (Marks et al., 2016, 2014). By weight, the gasifier biochar's particle sizes were largely in the 500–2000 mm (42%) and 50–100 mm (28%) fractions. The high production temperature promoted the relatively high ash content (for a wood biochar) 10.8±0.3%

69 and a carbon content of 79±1%.

70 Pine/TiO_2 was prepared following the synthesis described by *Kim and Kan* (2016) modified from
71 the synthesis initially described by *Wang et al.* (2008). Pine was washed with deionized water and
72 dried in an oven at 75 ºC for 24 h. After that, 5 g of this pre-treated pine were suspended in nitric
73 acid (65%) at pH 3.0 for 4 days as a conditioning procedure. This is necessary to ensure that the
74 functional groups of the carboxylic acid are in their protonated form to favor the heavy metal
75 adsorption process at pH 4.0. The acid conditioned Pine was filtrated from the acid solution and
76 washed with deionized water multiple times until neutral pH of the water was obtained. Then the
77 material was dried in an oven at 75 ºC for 24 h. The second stage comprise the synthesis of TiO_2 on
78 the Pine surface by sol-gel method. For that, 5.0 g acid treated Pine was dispersed in 120 ml ethanol
79 (97% v/v) followed by addition of 40 ml titanium(IV) butoxide (97%) used as TiO_2 precursor. The
80 mixture was stirred at ambient temperature for 1 h before adding a solution containing 16 ml of HCl
81 37% (v/v) and 40 ml ethanol (97% v/v) with constant stirring for 1 h more. The resultant material,
82 Pine/TiO_2, was filtered and washed with ethanol (97% v/v) before drying it at 70 ºC for 24 h. The
83 sample was milled and further dried at 325 ºC for 1 h in a muffle.

84 Both Pine and PG were also milled to achieve a comparable particle size (~10-100 μm) in order
85 to keep as similar as possible the experiment conditions for all sorbents.

86 **2.3 Characterization of materials**

87 The morphology of the sorbents was analyzed by scanning electron microscopy (SEM) at *Servei*
88 *de Microscòpia* of UAB (Barcelona, Spain) using a SEM ZEISS MERLIN. X-ray diffraction
89 measurements were performed on Pine/TiO_2 samples to characterize the phase of the TiO_2 particles
90 using an X-Pert Philips diffractometer (results and further details can be found in supplementary

information). BET technique (Micrometrics, TriStar II 3020, USA) was used to characterize the surface area and porosity. Prior to the mesoporous measurements, samples were heated at 200 °C for 4 h under vacuum. Zeta potential was used to analyze the surface charge of bio-sorbents (Malvern, ZEN 3600, USA). For the measurements, 100 mg of sample was mixed with 100 ml of water and the mixture was ultrasonicated for 10 minutes. pH was adjusted to 4.0 using HCl and NaOH. Triplicate measurements were performed, and each sample was measured 3 times to analyze the zeta potential values. BET and zeta potential measurements were performed at the Oil Crops Research Institute, OCRI (Wuhan, China). Attenuated total reflectance Fourier transform infrared (ATR-FTIR) spectroscopy was performed to identify the functional groups present in the adsorbents. FTIR was measured with an ATR-FTIR, Tensor 27 (Bruker) at *Servei d'Anàlisi de Química* of UAB (Barcelona, Spain) in the wavenumber range of 600 to 4000 cm^{-1} averaging 16 scans of 4.0 cm^{-1} resolution. The pH of the solid sorbents was determined as follows, 20 mg of sorbent was added to 1 ml of deionized water (1:50 ratio) and agitated vertically at 25 rpm over 24h. Then, the pH was measured immediately (Marks et al., 2014). This procedure was done three times and the mean value is reported.

2.4 Batch adsorption experiments

Adsorption experiments were carried out at room temperature (25±1 °C). Cr(III) and Cr(VI) solutions were prepared from 1000 mg/L initial stock solutions of each chromium species. The concentrations used ranged from 0 to 300 mg/L to consider chromium levels relevant for wastewater treatment applications (Wang et al., 2019). The pH was initially adjusted to pH 4.0 to avoid precipitation of Cr(III) as $Cr(OH)_3$ which occurs at higher pH. The study of the effect of the initial concentration on the adsorption capacity provides a significant understanding of both Cr metal ion

species during the adsorption process. Batch experiments were performed by mixing 25 mg of adsorbent and 2.5 ml of heavy metal aqueous solutions in 5 ml tubes. The tubes were then placed in a rotary mixer (CE 2000 ABT-4, SBS Instruments SA, Barcelona, Spain) and shaken at 25 rpm. From the contact time adsorption experiments, it was determined that the equilibrium was reached after 1h (see Figure S1 in the supporting information). For shake of simplicity and in order to compare with other materials, the adsorption experiments run over 24h. The sorbent phase was separated by filtration through 0.22 μm Millipore filters (Millex-GS, Millipore). The total concentration of chromium in the supernatant phase was analyzed by ICP-MS (XSERIES 2 ICP-MS, Thermo Scientific, USA). The concentration of Cr(VI) was determined by the colorimetric method based on 1,5-diphenylcarbazide (DPC) dye (Lace et al., 2019). The solution of 1,5-diphenylcarbazide was prepared by dissolving 250 mg of DPC 98% (Sigma Aldrich, Barcelona, Spain) in 50 mL acetone. The pH was adjusted to 2.0 adding the appropriated amount of phosphoric acid 85% v/v (Panreac, Barcelona, Spain). 50 μL of the prepared acid DPC solution were added to 50 μL of sample solution containing Cr(VI). The mixture was diluted with distilled water to 10 mL, shaken and left for 5 minutes to form the dyphenylcarbazone (DPCA) complex, Cr(III)-DPCA. The absorbance was measured at 540 nm. The Cr(III) concentration was calculated as the difference between the total Cr concentration determined by ICP-MS and the Cr(VI) concentration obtained by the colorimetric method.

The adsorption of each species was expressed as the adsorption percentage calculated using Equation (1), and the adsorption capacity of the adsorbent, q_e (mg/g), expressed as the amount of heavy metal per adsorbent mass unit at equilibrium was calculated using Equation (2):

$$\%\, Adsorption = \frac{(C_0 - C_e)}{C_0} \times 100 \qquad (1)$$

$$q_e = \frac{(C_0 - C_e) \times V}{m} \quad (2)$$

where V (L) is the volume of the heavy metal solution; C_0 and C_e (mg/L) are the initial and equilibrium heavy metal concentrations in the solution; and m (g) is the dry weight of the adsorbent. All the results are expressed as the mean value of a minimum of duplicate measurements.

2.5 Kinetics modelling

In order to evaluate the performance of the different sorbent materials, the kinetics of the adsorption process was characterized at an intermediate concentration of 9 mg/L of the different chromium species. The experimental conditions were similar to those detailed in Section 2.4. Four different models, pseudo-first-order (PFO), pseudo-second-order (PSO), Elovich and Intra-particle Diffusion (Qiu et al., 2009), were used to describe the adsorption kinetics of the different biosorbent systems. More details regarding the mathematical expressions of the models used and the experiment can be found in the supplementary information.

2.6 X-ray absorption spectroscopy study

For the XAS experiments, Pine, Pine/TiO_2 and PG samples were exposed to 349 and 470 mg/L single-element solutions of Cr(III) and Cr(VI), respectively, during 24 h in a rotary sacker at 25 rpm. Subsequently, the solids were separated from the solution by filtration and washed with milliQ water at room temperature (25±1 ºC) for 3 times to eliminate any remaining Cr solution and leave only the adsorbed Cr. Finally, the samples were dried in an oven at 70 ºC for 1 day. The dried powder was pressed into a pellet to facilitate its handling. XAS measurements were performed at the B18 beamline of the Diamond Light Source synchrotron facility (Didcot, United Kingdom) (Dent et al., 2009). EXAFS was collected at Cr K-edge using QEXAFS scanning mode and Si(111) monochromator crystals. The measurements were performed at liquid nitrogen temperature to

minimize possible radiation damage. Due to the low concentration of Cr in the samples, the measurements were performed in fluorescence mode using the 4-element Si-Drift detector available at the beamline. Reference samples (potassium dichromate(VI), Cr(III) acetate hydroxide, Cr(III) acetylacetonate, Cr(III) nitrate nonahydrate) were measured in transmission mode using gas ionization chambers filled with the appropriate amount of nitrogen and argon to absorb 15% (I_0) and 70% (I_t and I_{ref}) of the beam. XAS data analysis (i.e., spectra averaging, background subtraction, and spectra normalization) was performed according to standard procedures using the ATHENA program included in the Demeter software package (Ravel and Newville, 2005). The XANES spectra were rebinned to have a 0.5 eV energy grid in the edge region, between -40 and 120 eV respect to the edge position (E_0). The Fourier transform of the EXAFS signal was performed in the k-range 2.6 – 12.55 $Å^{-1}$.

3. Results and Discussion

3.1 Morphology, porosity and surface properties

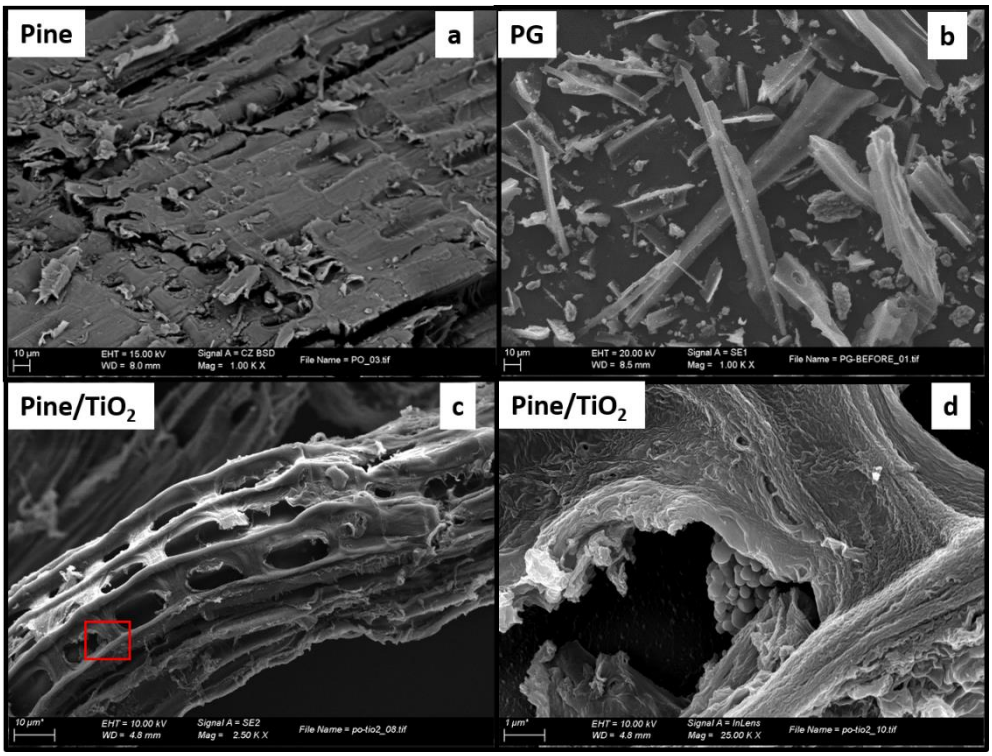

Figure 1. SEM images of Pine (a), PG (b), Pine/TiO_2 (c) at similar magnification (scale bar 10 µm); and Pine/TiO_2 (d) at higher magnification (scale bar 1 µm). Red square in panel c denotes the area of the image that is shown enlarged in panel d.

Table 1. BET and Zeta potential analysis of Pine, PG and Pine/TiO_2.

	Pine	Pine/TiO_2	PG
Surface Area (m^2/g)	1.52	36.1	128
Pore Volume (cm^3/g)	0.0177	0.0454	0.257
Pore Size (nm)	44.2	4.71	7.99
Zeta potential (mV) pH 4.0	-11.5	-20.3	-18.1

SEM images displayed in Figure 1 show that Pine has an irregular surface morphology that totally changes to more ordered graphene-type sheets after the pyrolysis treatment at high temperature to obtain PG, as expected. This is due to the degradation of cellulose, hemicellulose and lignin present in the original biomass material (Bagreev et al., 2001; Hossain et al., 2011; Sun et al., 2014; Zhao et al., 2017). As a result, the biochar material, PG, has a smoother surface and much smaller particle size than the original biomass, Pine. The BET results reported in Table 1 show that PG has much larger surface area and pore volume, and smaller pore size than Pine which demonstrates the increase in porosity after pyrolysis (Li et al., 2017). On the other side, Pine/TiO_2 shows quite similar

surface morphology than Pine, but with the addition of micro-sized TiO_2 particles as can be seen in Figure 1(d). The presence of TiO_2 was also confirmed by SEM-EDX measurements (see Figure S2 and S3). The loading of TiO_2 was very low as confirmed by the XRD measurements (see Figure S4). No appreciable diffraction peaks from TiO_2 particles were detected above the background level of the amorphous porous biomass structure. Since the temperature used to synthesize Pine/TiO_2 is low, 325 ^oC, most of the original components and characteristic structure of the original Pine material is preserved. The increase of surface area and pore volume, and the decrease of pore size could be attributed to the additional porosity associated with the micro-sized TiO_2 particles.

The zeta potential values at pH 4.0 are shown in Table 1. The zeta potential value for PG and Pine/TiO_2 is more negative than for Pine. This means that there is more negative charge on the surface of PG and Pine/TiO_2 than in Pine that may favor the interaction with heavy metal cations such as Cr^{3+}.

3.2 ATR-FTIR characterization

ATR-FTIR analysis was carried out to identify the functional groups present in the different sorbents that might be involved in the sorption process. FTIR spectra of Pine, Pine/TiO_2 and PG are shown in Figure 2. A decrease in the intensity of the bands corresponding to carboxyl (-COOH) and hydroxyl (-OH) groups is observed in the FTIR spectra of Pine/TiO_2 and PG after thermal treatments applied to Pine (see Table S1 for band assignments) (Larkin, 2011). Indeed, the FTIR of PG indicates the loss of most of the functional groups due to the pyrolysis of the lignocellulosic materials at high temperature. This is confirmed by the decrease of H/C and O/C atomic ratios of PG respect to Pine, from 1.33 to 0.19 and from 0.69 to 0.10, respectively (Marks et al., 2014). As reported by Al-Wabel *et al.* (2013), -COOH functional group decomposes at the high temperatures of the pyrolysis process,

being completely lost above 700 ºC. The reduction in concentration of functional groups such as -COOH, -COH and -OH after pyrolysis tends to increase the pH of the biochar sorbents (Li et al., 2017). Indeed, the pH value obtained for PG, pH 9.0, is much higher than for Pine and Pine/TiO_2, pH 6.0.

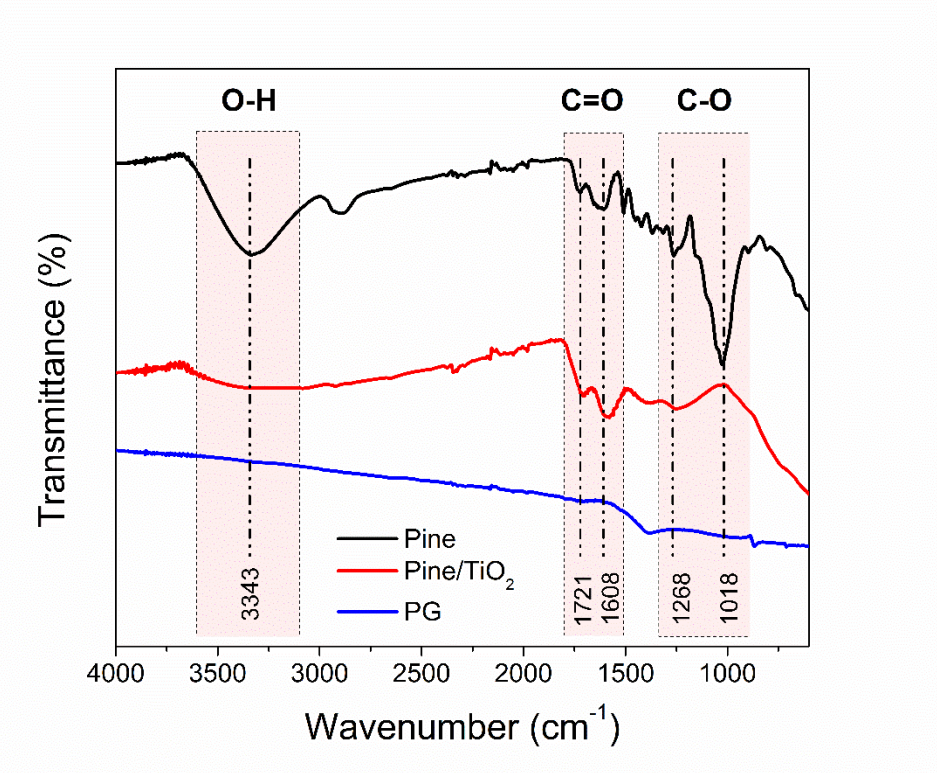

Figure 2. ATR-FTIR spectra of Pine, Pine/TiO_2 and PG.

3.3 Kinetics modelling

The analysis of the kinetics considering PFO, PSO and Elovich models (see Supporting Information and Figure S5) showed that all these models were suitable to describe the adsorption of both chromium species in all the biosorbent materials, with the exception of PG in contact with Cr(VI) (see Table S2). On the other hand, the Intra-particle Diffusion model did not reproduce in any case the adsorption behavior found. As the adsorption of chromium follows both PFO and PSO models, the adsorption of chromium on the surface of the adsorbents is probably due to a

combination of the physical and chemical adsorption process between the adsorbent and adsorbate, either via Van der Waals, covalent or ion exchange interactions as PSO kinetics is controlled by chemical processes, including valence forces sharing or exchanging electrons between the adsorbent and adsorbate as it has been previously described (Qiu et al., 2009). In the case of Cr(VI) adsorbed on PG, none of the selected models could successfully reproduce the trend since the adsorption is negligible in this case.

3.4 Comparison of biosorbent adsorption properties

The study of the effect of the initial concentration on the adsorption capacity (see Figure S6) showed that neither PG for Cr(III) or Pine/TiO_2 for Cr(VI) reached saturation within the concentration range used and pH 4.0. When comparing the adsorption capacity of Cr measured for the three sorbent materials remarkable differences are found depending on the chromium species present in solution, Cr(III) or Cr(VI), see Figure 3. Although both, Pine and Pine/TiO_2, have better sorption capacity of Cr(VI) than for Cr(III), an enhancement of this sorption capacity is found for Pine/TiO_2 respect to Pine for both Cr species, especially for Cr(VI). However, PG outperforms both of them in the case of Cr(III) adsorption, whereas it displays negligible adsorption of Cr(VI). The main factors influencing the adsorption of heavy metals are expected to be functional groups, pH of the sorbent, mineral elements content (e.g. K, Ca, Mg and P) and specific surface area (Chen et al., 2018; Wnetrzak et al., 2014; Yuan et al., 2011). In our case, the mineral element concentration values for PG are much larger than for Pine (9.36 and 0.68 mg/kg for K, 20.5 and 0.67 mg/kg for Ca, 2.1 and 0.15 mg/kg for Mg, and 1.3 and 0.07 mg/kg for total P content in PG and Pine, respectively) (Marks et al., 2014). This is due to the fact that these mineral elements are concentrated on the surface of the adsorbent during the pyrolysis process at high temperature. During that process, most

242 of the organic matter of the biomass is pyrolyzed, thus increasing the relative concentration of
243 mineral elements in the material. The cation exchange capacity (CEC) reported for PG was 21 ± 7
244 $mmol_c/kg$ (Marks et al., 2016) which is low when comparing with other better performing biochars,
245 but much larger than wood biomass materials. Furthermore, due to its negative surface, PG can
246 easily attract positive cations as Cr^{3+}, which can be exchanged with the K^+, Ca^{2+} and Mg^{2+} cations
247 (Wnetrzak et al., 2014). Thus, the negative charge and the larger specific surface of PG can explain
248 its enhanced adsorption capacity for Cr(III) over Pine and Pine/TiO_2. Following a similar reasoning,
249 the higher Cr(III) removal efficiency of Pine/TiO_2 over Pine can be ascribed to its higher surface
250 area (see Table 1) and to the slightly increase of the mineral element content after the low
251 temperature thermal treatment since still an important amount of organic matter from the original
252 Pine biomass remains in the Pine/TiO_2 sorbent.
253 Regarding Cr(VI), since it is found in aqueous solution at pH 4.0 as chromate anion, $HCrO_4^-$
254 (Markiewicz et al., 2015), it will not interact neither with carboxyl neither with hydroxyl functional
255 groups present in the sorbents studied. Even though, at low pH, only the interaction with lignin
256 could facilitate the adsorption of Cr(VI) by Pine due to the fact that the surface of lignin carries less
257 negative charges and it can readily adsorb the chromate anion by physical and/or Van der Waals
258 interactions (Chen et al., 2018; Wang et al., 2019). The enhanced adsorption of Cr(VI) found in
259 Pine/TiO_2 respect to Pine can be attributed to the micro-sized TiO_2 particles due to the presence of
260 $TiOH_2^+$ groups, which dominate for pH below 4.2 (Weng et al., 1997). Indeed, since the loading of
261 the TiO_2 particles on the surface is small, it should cover only a small surface area of the Pine/TiO_2
262 material. Thus, most of the surface is composed by the low temperature pyrolyzed biochar support.
263 The negatively charged surface of the support can explain that Pine/TiO_2 has a much negative value

of the Zeta potential that the original Pine biomass. In the case of PG, there is a larger amount of minerals cation elements concentrated on the surface than the amount of $TiOH_2^+$ groups present in the Pine/TiO_2 sorbent material. Therefore, Pine/TiO_2 has less amount of mineral cation content than PG and just a relatively small amount of $TiOH_2^+$ groups, which in global leads to a more negative surface charge (or zeta potential measurement) in comparison with PG. Regarding PG, its negligible Cr(VI) adsorption can be understood by the electrostatic repulsion between chromate and OH^- groups expected to be present in the PG surface due to the higher pH of the adsorbent (pH 9.0) that increases the competition with OH^-.

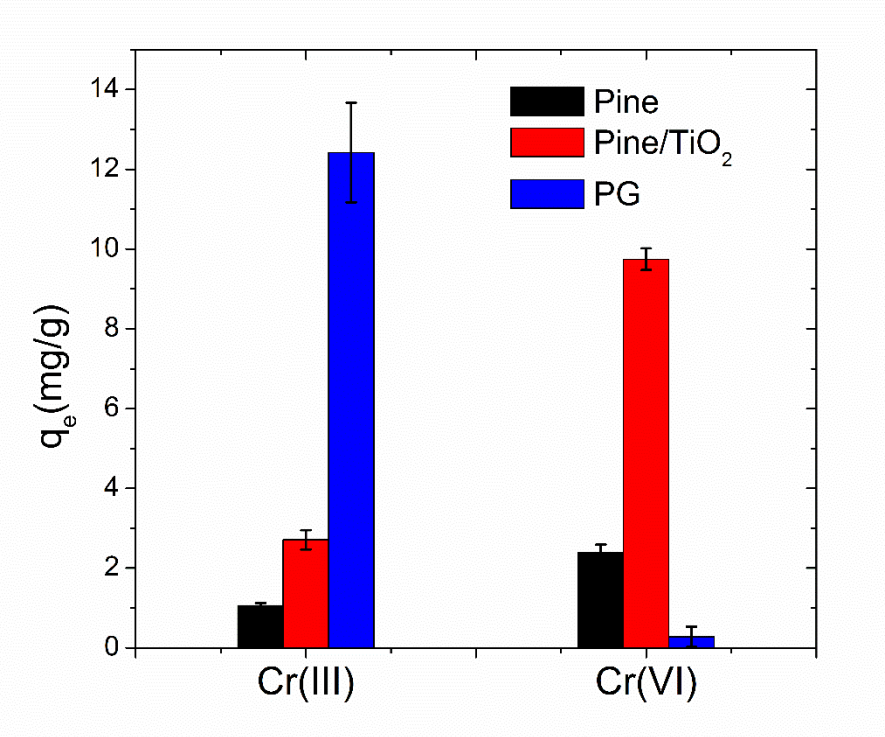

Figure 3. Adsorption capacity of Cr for Pine, Pine/TiO_2 and PG for an initial metal concentration of 120 mg/L.

3.5 Adsorption isotherm modelling

The Cr(III) and Cr(VI) adsorption isotherms for the three sorbents are shown in panels (a) and (b) of Figure 4, respectively. Langmuir and Freundlich isotherm models were used to understand the adsorption mechanism for the interaction of heavy metal ions on the adsorbent surface. Langmuir

model assumes that the uptake of metal ions occurs on a homogeneous surface by a monolayer deposition, whereas Freundlich isotherm model is employed to describe the equilibrium process on a heterogeneous surface. See supplementary information for further details.

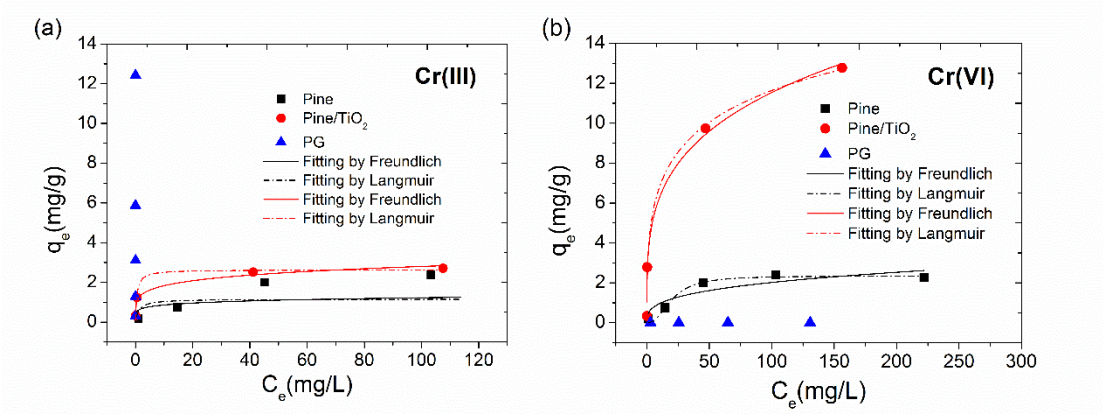

Figure 4. Adsorption isotherms for Pine, Pine/TiO_2 and PG measured at T=25±1ºC: Cr(III) (a); and Cr(VI) (b). Freundlich model (continuous line) and Langmuir model (dot and dash line) are shown for each curve.

Adsorption isotherms for Pine/TiO_2 are well described either by Freundlich and Langmuir models for both Cr(III) and Cr(VI) as displayed in Figure 4a and 4b, respectively. The final parameters of the modelling are shown in Table 2. For Pine, Langmuir model describes noticeably better the experimental data for both chromium species. On another hand, the Cr(III) isotherm for PG does not reach saturation due to its high adsorption capacity even when reaching 300 mg/L of the initial concentration. In the case of Cr(VI), PG shows quite low adsorption capacity which is not reproduced by any model.

The results obtained for Pine/TiO_2 can be understood considering the actual nature of the sorbent material itself. The agreement with the Freundlich model describes the adsorption equilibrium process on its heterogeneous surface. Moreover, the good agreement also achieved with the Langmuir model suggests that there is a monolayer interaction between the chromium species and

the sorbent surface. As shown in Table 2, both models provide a maximum adsorption capacity of both Cr species for Pine/TiO_2 much larger than the original biomass material, Pine. On the other side, since Pine is more homogeneous than Pine/TiO_2, a monolayer deposition on its surface explains the adsorption process of chromium following Langmuir model. That behavior can also be related to the proposed adsorption mechanisms for both chromium species, being the metal ion-exchange interaction with functional groups for Cr(III), and the Van der Waals interaction with the lignin structure for Cr(VI).

Table 2. Results from fitting the isotherm measurements to Langmuir and Freundlich models.

		Langmuir			**Freundlich**			
		q_{max} (mg/g)	K_L (L/mg)	R^2	$q_{e,max}$ (mg/g)	K_f ((mg/g)·(L/mg)$^{1/n}$)	n	R^2
Cr(III)	Pine	1.14	0.838	0.951	1.16	0.605	0.154	0.616
	Pine/TiO_2	2.83	1.15	0.996	1.23	1.20	0.184	0.941
Cr(VI)	Pine	2.35	0.001	0.974	2.26	0.454	0.324	0.784
	Pine/TiO_2	27.0	0.149	0.975	12.8	3.40	0.266	0.982

3.6 X-ray absorption spectroscopy study

XAS was used to investigate the interaction of the heavy metal with the different adsorption sites present in the surface of Pine, Pine/TiO_2 and PG. The XAS spectrum can be divided in two characteristic regions: X-ray absorption near-edge spectroscopy (XANES) and extended X-ray absorption fine-structure spectroscopy (EXAFS). XANES, which is closer to the absorption edge, is sensitive to formal oxidation state and coordination chemistry of the probed element, while EXAFS is used to determine the distances, coordination number, and species of neighbors of the probed element. Figure 5 shows the comparison of the Cr K-edge XANES spectra of the sorbent materials with the Cr reference compounds. The spectrum of potassium dichromate reference

315 compound, in which Cr is tetrahedrally coordinated (Td) with four oxygens, is characterized by an
316 intense pre-peak that can be assigned to a partially allowed dipole transition due to the mixture of
317 states produced by the lack of inversion center (Peterson et al., 1996). On the other hand, a much
318 less intense pre-edge feature is found in the spectra of the Cr(III) references in which chromium is
319 coordinated with 6 ligands in a distorted octahedral configuration. As expected, the absorption edge
320 of the chromate reference is shifted towards higher energy respect to the Cr(III) references.
321 The most striking fact is that the sorbent samples exposed to Cr(VI) solution do not show the
322 characteristic and intense pre-edge feature of chromate species. The only sample showing a hint of
323 the chromate pre-peak feature is PG-Cr(VI). The reduction of the chromate in the solution during
324 the adsorption process can be discarded since the concentration of the Cr(VI) species was checked
325 using UV-Vis spectroscopy before and after the adsorption experiment.

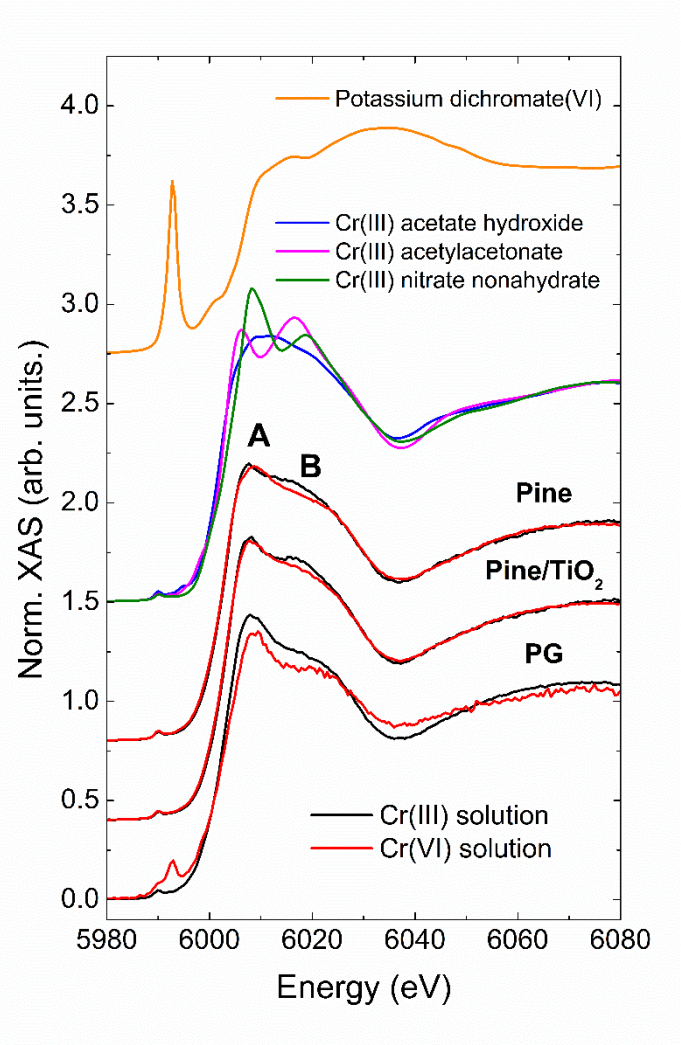

Figure 5. XAS spectra at Cr K-edge for Cr references and Pine, PG and Pine/TiO_2 sorbent materials after adsorbing Cr(III) and Cr(VI).

Indeed, the spectral profile of the samples exposed to Cr(VI) is quite similar to the Cr(III) ones. The only difference between the two different Cr species is found in the profile of the white-line (main resonance after the absorption edge). The feature B in the XANES spectra of the Pine and Pine/TiO_2 is slightly more intense for Cr(III) adsorption than for Cr(VI). This might be ascribed to the slightly distorted environment of Cr atom that can be found in the case of Cr(VI) adsorption-reduction mechanism.

Regarding the EXAFS signal displayed in Figure 6, there is a clear difference of the spectra collected on the Cr(III) references respect to the Cr(VI) ones. The main difference is the higher

frequency of the main oscillation in the Cr(III) EXAFS signal (panel a) which reflects the larger Cr-O distance of the distorted octahedral arrangement of Cr(III) respect to the tetrahedral one of the chromate (Cr(VI)). This can be appreciated more clearly in the pseudo-radial distribution function in the real space (R) after applying the Fourier Transform (panel b). In accordance with the XANES results, all the sorbent samples show a similar spectral profile regardless the Cr species exposed to. The only one which is slightly different is the PG-Cr(VI) sample that, as it has been mentioned, it contains a mixture of Cr(VI) and Cr(III).

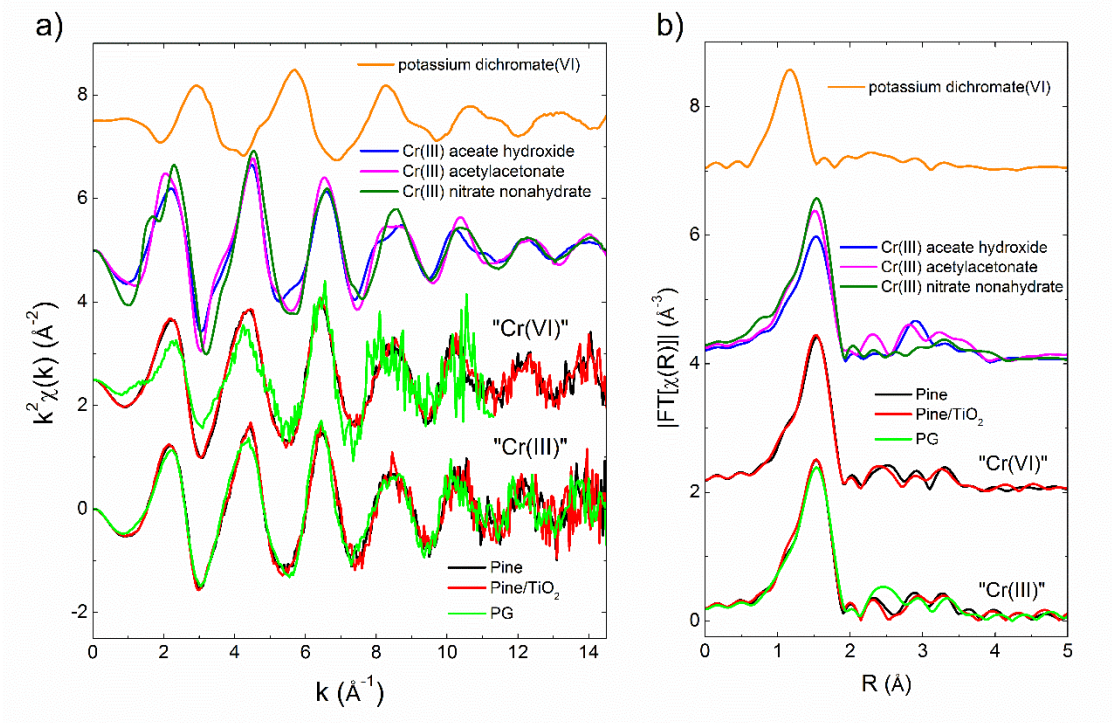

Figure 6. EXAFS signal (a) and pseudo-radial distribution function (b) at Cr K-edge for Cr references and Cr-loaded on Pine, PG and Pine/TiO_2 sorbent materials.

In order to get a better insight on the character of the Cr adsorbed on the different materials, a linear combination fitting analysis of the XANES spectra of the samples using the four Cr references was performed. The results shown in the supporting information (Table S3) confirmed the absence of Cr(VI) in Pine-Cr(VI) and Pine/TiO_2-Cr(VI), and the presence of ~18% of chromate in PG-Cr(VI). This observation suggests that the adsorption of the chromate occurs before its reduction. On the

352 contrary, the occurrence of the reduction step before the adsorption would imply a much larger
353 adsorption capacity of PG-Cr(VI) as found for PG-Cr(III). The little amount of Cr(VI) detected in
354 PG might be residual traces of the initial Cr(VI) solution that were not properly washed out from
355 the sorbent material after the adsorption experiment when rinsing the solid sorbent. The adsorption-
356 reduction mechanism has been interpreted by other authors working with biochar as a two-step
357 process. First, the Cr(VI) ions are electrostatically attracted by the few remaining positively charged
358 functional groups. Biochar produced at higher pyrolysis temperatures, which has more well-ordered
359 graphene sheets, is expected to be a better donator of π-electrons (Uchimiya et al., 2011). These π-
360 electrons are a likely source of electrons for reducing Cr(VI) to Cr(III). Finally, Cr(III) is retained
361 on the PG sorbent material by the few amount of negatively charged groups (Rajapaksha et al., 2018;
362 Xu et al., 2019). However, this mechanism cannot account for the adsorption/reduction mechanism
363 occurring in Pine and Pine/TiO_2 samples. In biomass, it has been proposed that oxygen containing
364 groups, such as carboxyl and phenolic groups, play a major role in the binding of the Cr(III) resulting
365 from the abiotic reduction of Cr(VI) by the biomass (Park et al., 2008). These surface functional
366 groups, which are abundant on Pine and Pine/TiO_2, might serve as the electron donating moiety to
367 provide the electrons for the Cr(VI) reduction. Regarding Pine/TiO_2, our results suggest that the
368 interaction between $TiOH_2^+$ and the chromate anion occurs through hydrogen bonding since no
369 titanium contribution has been found in the second coordination shell of the pseudo-radial
370 distribution function of the EXAFS signal (Figure 6b) measured on Pine/TiO2-Cr(VI). The presence
371 of that contribution would be linked to the occurrence of Cr-O-Ti bonding structures.
372
373

4. Conclusions

In this work, we describe the molecular adsorption mechanisms of Cr(III) and Cr(VI) by Pine, PG and Pine/TiO_2 to explain the Cr species-dependent enhanced adsorption observed in the modified biomass materials via either gasification or by loading TiO_2 particles, for Cr(III) and Cr(VI), respectively. The enhanced adsorption of Cr(III) in PG respect to Pine can be mostly attributed to the high number of the cation mineral elements concentrated on the large surface area obtained after pyrolysis that can promote their exchange processes with Cr(III), since the negatively charged surface of the PG sorbent can favor the attraction of positive cations such as Cr^{3+}. In the case of Pine/TiO_2, the presence of $TiOH_2^+$ groups enhances the adsorption Cr(VI) as $HCrO_4^-$. In addition, we have observed that the highly toxic and carcinogenic Cr(VI) gets reduced to the less toxic Cr(III) in the case of Pine or Pine/TiO_2 which is highly desirable for the treatment of Cr(VI)-contaminated waters.

This demonstrates that biomass-based sorbents are an interesting, cost-effective and eco-friendly alternative to traditional polymeric and inorganic synthetic materials that are nowadays used for heavy metal removal. For possible large-scale applications, the synthesis procedure of Pine/TiO_2 composite material should be thoroughly reviewed and optimized to obtain competitive commercial materials. Furthermore, the valorization of such biomass residues can help our society to become more sustainable while the best performance can be achieved in practical applications for water remediation.

Acknowledgements

This research was supported by grants from Spanish research projects (CTM2015-65414-C2-1-

R and AGL2015-70393-R) and China Scholarship Council (201509110114). We acknowledge Diamond Light Source facility for beamtime SP18561 at B18 beamline and funding received from them to cover the trip and stay in UK. The synchrotron experiment has been supported by the project CALIPSOplus under the Grant Agreement 730872 from the EU Framework Programme for Research and Innovation Horizon 2020. R.B. acknowledges funding support from the European Union's Horizon 2020 research and innovation program under the Marie Skłodowska-Curie grant agreement No. 665919. All the authors are grateful to the UAB Microscopy Service (*Servei de Microscòpia Electrònica* from UAB, Catalunya, Spain) for the SEM analysis.

References

Al-Wabel, M.I., Al-Omran, A., El-Naggar, A.H., Nadeem, M., Usman, A.R.A., 2013. Pyrolysis temperature induced changes in characteristics and chemical composition of biochar produced from conocarpus wastes. Bioresour. Technol. 131, 374–379. https://doi.org/10.1016/j.biortech.2012.12.165

Álvarez-Álvarez, P., Pizarro, C., Barrio-Anta, M., Cámara-Obregón, A., María Bueno, J.L., Álvarez, A., Gutiérrez, I., Burslem, D.F.R.P., 2018. Evaluation of tree species for biomass energy production in Northwest Spain. Forests 9, 1–15. https://doi.org/10.3390/f9040160

Bagreev, A., Bandosz, T.J., Locke, D.C., 2001. Pore structure and surface chemistry of adsorbents obtained by pyrolysis of sewage sludge-derived fertilizer. Carbon N. Y. 39, 1971–1979. https://doi.org/10.1016/S0008-6223(01)00026-4

Braghiroli, F.L., Passarini, L., 2020. Valorization of Biomass Residues from Forest Operations and Wood Manufacturing Presents a Wide Range of Sustainable and Innovative Possibilities. Curr. For. Reports 6, 172–183. https://doi.org/10.1007/s40725-020-00112-9

Chen, Y., Wang, B., Xin, J., Sun, P., Wu, D., 2018. Adsorption behavior and mechanism of Cr(VI) by modified biochar derived from Enteromorpha prolifera. Ecotoxicol. Environ. Saf. 164, 440–447. https://doi.org/10.1016/j.ecoenv.2018.08.024

Demirbas, A., 2008. Heavy metal adsorption onto agro-based waste materials: A review. J. Hazard. Mater. 157, 220–229. https://doi.org/10.1016/j.jhazmat.2008.01.024

Dent, A.J., Cibin, G., Ramos, S., Smith, A.D., Scott, S.M., Varandas, L., Pearson, M.R., Krumpa, N.A., Jones, C.P., Robbins, P.E., 2009. B18: A core XAS spectroscopy beamline for Diamond. J. Phys. Conf. Ser. 190. https://doi.org/10.1088/1742-6596/190/1/012039

Gode, F., Atalay, E.D., Pehlivan, E., 2008. Removal of Cr(VI) from aqueous solutions using modified red pine sawdust. J. Hazard. Mater. 152, 1201–1207. https://doi.org/10.1016/j.jhazmat.2007.07.104

GracePavithra, K., Jaikumar, V., Kumar, P.S., SundarRajan, P.S., 2019. A review on cleaner strategies for

chromium industrial wastewater: Present research and future perspective. J. Clean. Prod. 228, 580–593. https://doi.org/10.1016/j.jclepro.2019.04.117

Heredia Salgado, M.A., Coba S, J.A., Tarelho, L.A.C., 2020. Simultaneous production of biochar and thermal energy using palm oil residual biomass as feedstock in an auto-thermal prototype reactor. J. Clean. Prod. 266. https://doi.org/10.1016/j.jclepro.2020.121804

Hossain, M.K., Strezov Vladimir, V., Chan, K.Y., Ziolkowski, A., Nelson, P.F., 2011. Influence of pyrolysis temperature on production and nutrient properties of wastewater sludge biochar. J. Environ. Manage. 92, 223–228. https://doi.org/10.1016/j.jenvman.2010.09.008

Hu, J., Shipley, H.J., 2013. Regeneration of spent TiO2 nanoparticles for Pb (II), Cu (II), and Zn (II) removal. Environ. Sci. Pollut. Res. 20, 5125–5137. https://doi.org/10.1007/s11356-013-1502-7

Inyang, M., Gao, B., Yao, Y., Xue, Y., Zimmerman, A.R., Pullammanappallil, P., Cao, X., 2012. Removal of heavy metals from aqueous solution by biochars derived from anaerobically digested biomass. Bioresour. Technol. 110, 50–56. https://doi.org/10.1016/j.biortech.2012.01.072

Jobby, R., Jha, P., Yadav, A.K., Desai, N., 2018. Biosorption and biotransformation of hexavalent chromium [Cr(VI)]: A comprehensive review. Chemosphere 207, 255–266. https://doi.org/10.1016/j.chemosphere.2018.05.050

Kim, J.R., Kan, E., 2016. Heterogeneous photocatalytic degradation of sulfamethoxazole in water using a biochar-supported TiO2 photocatalyst. J. Environ. Manage. 180, 94–101. https://doi.org/10.1016/j.jenvman.2016.05.016

Lace, A., Ryan, D., Bowkett, M., Cleary, J., 2019. Chromium monitoring in water by colorimetry using optimised 1,5-diphenylcarbazide method. Int. J. Environ. Res. Public Health 16. https://doi.org/10.3390/ijerph16101803

Larkin, P., 2011. Infrared and Raman Spectroscopy: Principles and Spectral Interpretation, Infrared and Raman Spectroscopy. Elsevier.

Li, H., Dong, X., da Silva, E.B., de Oliveira, L.M., Chen, Y., Ma, L.Q., 2017. Mechanisms of metal sorption by biochars: Biochar characteristics and modifications. Chemosphere 178, 466–478. https://doi.org/10.1016/j.chemosphere.2017.03.072

Littlejohns, J. V., Butler, J., Luque, L., Austin, K., 2020. Experimental Investigation of Bioenergy Production from Small-Scale Gasification of Landfill-Diverted Wood Wastes. Waste and Biomass Valorization. https://doi.org/10.1007/s12649-020-00940-7

Markiewicz, B., Komorowicz, I., Sajnóg, A., Belter, M., Barałkiewicz, D., 2015. Chromium and its speciation in water samples by HPLC/ICP-MS - Technique establishing metrological traceability: A review since 2000. Talanta 132, 814–828. https://doi.org/10.1016/j.talanta.2014.10.002

Marks, E.A.N., Mattana, S., Alcañiz, J.M., Domene, X., 2014. Biochars provoke diverse soil mesofauna reproductive responses inlaboratory bioassays. Eur. J. Soil Biol. 60, 104–111. https://doi.org/10.1016/j.ejsobi.2013.12.002

Marks, E.A.N., Mattana, S., Alcañiz, J.M., Pérez-Herrero, E., Domene, X., 2016. Gasifier biochar effects on nutrient availability, organic matter mineralization, and soil fauna activity in a multi-year Mediterranean trial. Agric. Ecosyst. Environ. 215, 30–39. https://doi.org/10.1016/j.agee.2015.09.004

Miretzky, P., Cirelli, A.F., 2010. Cr(VI) and Cr(III) removal from aqueous solution by raw and modified lignocellulosic materials: A review. J. Hazard. Mater. 180, 1–19. https://doi.org/10.1016/j.jhazmat.2010.04.060

Nath, K., Kumar, N., 1988. Hexavalent chromium: Toxicity and its impact on certain aspects of

carbohydrate metabolism of the freshwater teleost, Colisa fasciatus. Sci. Total Environ. 72, 175–181. https://doi.org/10.1016/0048-9697(88)90016-2

Park, D., Yun, Y.S., Park, J.M., 2008. XAS and XPS studies on chromium-binding groups of biomaterial during Cr(VI) biosorption. J. Colloid Interface Sci. 317, 54–61. https://doi.org/10.1016/j.jcis.2007.09.049

Pellerin, C., Booker, S.M., 2000. Reflections on hexavalent chromium: Health hazards of an industrial heavyweight. Environ. Health Perspect. 108, A402-7. https://doi.org/10.2307/3434980

Peterson, M.L., Brown, G.E., Parks, G.A., 1996. Direct XAFS evidence for heterogeneous redox reaction at the aqueous chromium/magnetite interface. Colloids Surfaces A Physicochem. Eng. Asp. 107, 77–88. https://doi.org/10.1016/0927-7757(95)03345-9

Pradhan, D., Sukla, L.B., Sawyer, M., Rahman, P.K.S.M., 2017. Recent bioreduction of hexavalent chromium in wastewater treatment: A review. J. Ind. Eng. Chem. 55, 1–20. https://doi.org/10.1016/j.jiec.2017.06.040

Qiu, H., Lv, L., Pan, B.C., Zhang, Q.J., Zhang, W.M., Zhang, Q.X., 2009. Critical review in adsorption kinetic models. J. Zhejiang Univ. Sci. A 10, 716–724. https://doi.org/10.1631/jzus.A0820524

Rajapaksha, A.U., Alam, M.S., Chen, N., Alessi, D.S., Igalavithana, A.D., Tsang, D.C.W., Ok, Y.S., 2018. Removal of hexavalent chromium in aqueous solutions using biochar: Chemical and spectroscopic investigations. Sci. Total Environ. 625, 1567–1573. https://doi.org/10.1016/j.scitotenv.2017.12.195

Ravel, B., Newville, M., 2005. ATHENA, ARTEMIS, HEPHAESTUS: Data analysis for X-ray absorption spectroscopy using IFEFFIT. J. Synchrotron Radiat. 12, 537–541. https://doi.org/10.1107/S0909049505012719

Ray, P.Z., Shipley, H.J., 2015. Inorganic nano-adsorbents for the removal of heavy metals and arsenic: A review. RSC Adv. 5, 29885–29907. https://doi.org/10.1039/c5ra02714d

Sarin, V., Singh, T.S., Pant, K.K., 2006. Thermodynamic and breakthrough column studies for the selective sorption of chromium from industrial effluent on activated eucalyptus bark. Bioresour. Technol. 97, 1986–1993. https://doi.org/10.1016/j.biortech.2005.10.001

Sterritt, R.M., Lester, J.N., 1984. Significance and behaviour of heavy metals in waste water treatment processes III. Speciation in waste waters and related complex matrices. Sci. Total Environ. 34, 117–141. https://doi.org/10.1016/0048-9697(84)90045-7

Sun, Y., Gao, B., Yao, Y., Fang, J., Zhang, M., Zhou, Y., Chen, H., Yang, L., 2014. Effects of feedstock type, production method, and pyrolysis temperature on biochar and hydrochar properties. Chem. Eng. J. 240, 574–578. https://doi.org/10.1016/j.cej.2013.10.081

Tan, X., Liu, Y., Zeng, G., Wang, X., Hu, X., Gu, Y., Yang, Z., 2015. Application of biochar for the removal of pollutants from aqueous solutions. Chemosphere 125, 70–85. https://doi.org/10.1016/j.chemosphere.2014.12.058

Uchimiya, M., Chang, S.C., Klasson, K.T., 2011. Screening biochars for heavy metal retention in soil: Role of oxygen functional groups. J. Hazard. Mater. 190, 432–441. https://doi.org/10.1016/j.jhazmat.2011.03.063

Wan Ngah, W.S., Hanafiah, M.A.K.M., 2008. Removal of heavy metal ions from wastewater by chemically modified plant wastes as adsorbents: A review. Bioresour. Technol. 99, 3935–3948. https://doi.org/10.1016/j.biortech.2007.06.011

Wang, B., Sun, Y.-C., Sun, R.-C., 2019. Fractionational and structural characterization of lignin and its modification as biosorbents for efficient removal of chromium from wastewater: a review. J.

519 Leather Sci. Eng. 1, 1–25. https://doi.org/10.1186/s42825-019-0003-y
520 Wang, S., Ji, L.J., Wu, B., Gong, Q., Zhu, Y., Liang, J., 2008. Influence of surface treatment on preparing
521 nanosized TiO 2 supported on carbon nanotubes. Appl. Surf. Sci. 255, 3263–3266.
522 https://doi.org/10.1016/j.apsusc.2008.09.031
523 Wang, X., Pehkonen, S.O., Ray, A.K., 2004. Removal of Aqueous Cr(VI) by a Combination of
524 Photocatalytic Reduction and Coprecipitation. Ind. Eng. Chem. Res. 43, 1665–1672.
525 https://doi.org/10.1021/ie030580j
526 Weng, C.H., Wang, J.H., Huang, C.P., 1997. Adsorption of Cr(VI) onto TiO2 from dilute aqueous
527 solutions. Water Sci. Technol. 35, 55–62. https://doi.org/10.1016/S0273-1223(97)00114-5
528 Wnetrzak, R., Leahy, J.J., Chojnacka, K.W., Saeid, A., Novotny, E., Jensen, L.S., Kwapinski, W., 2014.
529 Influence of pig manure biochar mineral content on Cr(III) sorption capacity. J. Chem. Technol.
530 Biotechnol. 89, 569–578. https://doi.org/10.1002/jctb.4159
531 Xu, Z., Xu, X., Tao, X., Yao, C., Tsang, D.C.W., Cao, X., 2019. Interaction with low molecular weight
532 organic acids affects the electron shuttling of biochar for Cr(VI) reduction. J. Hazard. Mater. 378,
533 120705. https://doi.org/10.1016/j.jhazmat.2019.05.098
534 Yuan, J.H., Xu, R.K., Zhang, H., 2011. The forms of alkalis in the biochar produced from crop residues
535 at different temperatures. Bioresour. Technol. 102, 3488–3497.
536 https://doi.org/10.1016/j.biortech.2010.11.018
537 Zhao, J.J., Shen, X.J., Domene, X., Alcañiz, J.M., Liao, X., Palet, C., 2019. Comparison of biochars
538 derived from different types of feedstock and their potential for heavy metal removal in multiple-
539 metal solutions. Sci. Rep. 9, 1–12. https://doi.org/10.1038/s41598-019-46234-4
540 Zhao, S.X., Ta, N., Wang, X.D., 2017. Effect of temperature on the structural and physicochemical
541 properties of biochar with apple tree branches as feedstock material. Energies 10.
542 https://doi.org/10.3390/en10091293
543